Gelsolin mediates calcium-dependent disassembly of *Listeria* actin tails

Laura Larson*, Serge Arnaudeau†, Bruce Gibson*, Wei Li*, Ryoko Krause‡, Binghua Hao*, James R. Bamburg§, Daniel P. Lew‡, Nicolas Demaurex†, and Frederick Southwick*¶

*Department of Medicine, Division of Infectious Diseases, University of Florida College of Medicine, Gainesville, FL 32610; †Departments of Physiology and ‡Medicine/Infectious Diseases, University of Geneva, 1211 Geneva, Switzerland; and §Departments of Biochemistry and Molecular Biology, Colorado State University, Fort Collins, CO 80523

The role of intracellular Ca^{2+} in the regulation of actin filament assembly and disassembly has not been clearly defined. We show that reduction of intracellular free Ca^{2+} concentration ($[Ca^{2+}]_i$) to <40 nM in *Listeria monocytogenes*-infected, EGFP–actin-transfected Madin–Darby canine kidney cells results in a 3-fold lengthening of actin filament tails. This increase in tail length is the consequence of marked slowing of the actin filament disassembly rate, without a significant change in assembly rate. The Ca^{2+}-sensitive actin-severing protein gelsolin concentrates in the *Listeria* rocket tails at normal resting $[Ca^{2+}]_i$ and disassociates from the tails when $[Ca^{2+}]_i$ is lowered. Reduction in $[Ca^{2+}]_i$ also blocks the severing activity of gelsolin, but not actin-depolymerizing factor (ADF)/cofilin microinjected into *Listeria*-infected cells. In *Xenopus* extracts, *Listeria* tail lengths are also calcium-sensitive, markedly shortening on addition of calcium. Immunodepletion of gelsolin, but not *Xenopus* ADF/cofilin, eliminates calcium-sensitive actin-filament shortening. *Listeria* tail length is also calcium-insensitive in gelsolin-null mouse embryo fibroblasts. We conclude that gelsolin is the primary Ca^{2+}-sensitive actin filament recycling protein in the cell and is capable of enhancing *Listeria* actin tail disassembly at normal resting $[Ca^{2+}]_i$ (145 nM). These experiments illustrate the unique and complementary functions of gelsolin and ADF/cofilin in the recycling of actin filaments.

actin-based motility | actin-depolymerizing factor/cofilin

Despite more than two decades of study, the role of calcium in regulating the actin cytoskeleton in nonmuscle cells has not been clearly defined. In 1979 the first calcium-sensitive actin-regulatory protein, gelsolin, was described (1). Subsequently, numerous other calcium-sensitive actin-binding proteins have been discovered (2, 3). Studies of polymorphonuclear leukocytes revealed that stimulation by chemoattractants induced rapid actin filament assembly followed by slower disassembly (4–7). The rise in actin filament content was accompanied by a rise in cytoplasmic ionized calcium (8). These observations raised the possibility that calcium might play a critical role in chemoattractant-induced actin assembly and disassembly. However, subsequently, chelation of intracellular calcium was found to minimally affect chemoattractant-associated changes in polymorphonuclear leukocyte actin filament content (9, 10). Similarly, the changes in actin filament content associated with phagocytic stimuli proved to be minimally affected by reductions in intracellular calcium (11). These observations called into question the importance of intracellular calcium in regulating actin assembly and disassembly. However, subsequent studies in platelets revealed that reductions in intracellular calcium impaired the formation of lamellipodia, supporting a role for calcium in actin-based motility (12).

In addition to generating the shape changes for chemotaxis, phagocytosis, and spreading, actin assembly and disassembly play a critical role in the ability of several intracellular pathogens to move within host cells and spread from cell to cell (13). The dynamic changes in the actin cytoskeleton have been extensively studied in *Listeria monocytogenes*-infected tissue culture cells and cell extracts, and actin-based motility has been shown to be critical for *Listeria* pathogenesis. Although a rise in intracellular calcium is associated with enhanced phagocytosis of *Listeria* (14, 15), once the bacterium enters the cytoplasm, G proteins and calcium are not thought to play a role in *Listeria* actin-based motility (16).

The ability to assess the assembly and disassembly rates of *Listeria* actin tails make *Listeria* intracellular infection a simpler model system for reexamining the effects of calcium on the *in vivo* dynamics of actin filament formation. *Listeria* induces the assembly of new actin filaments at its rear surface. Because the older regions of the *Listeria* actin tail remain anchored in the cytoplasm, elongation of new filaments generates directional forces that drive the bacterium through the cytoplasm (17, 18), and the velocity of intracellular movement reflects the rate of new actin filament assembly (18, 19). Studies using fluorescently labeled actin reveal that the *Listeria* actin tails also steadily disassemble. The rate of tail disassembly is not affected by the velocity of bacterial movement, having a constant half-life of 40–60 s (18, 19). *Listeria* actin tail length reflects the sum of the assembly and disassembly rates, and the tails are longer in faster-moving bacteria or under conditions that slow actin tail disassembly.

In this study, we show that lowering intracellular free Ca^{2+} concentration ($[Ca^{2+}]_i$) causes a dramatic lengthening of *Listeria* actin tails because of a marked reduction in actin filament disassembly rate. Our experiments support a primary role for gelsolin in calcium-sensitive actin filament recycling. Furthermore, we find that gelsolin-induced actin filament disassembly occurs at normal resting $[Ca^{2+}]_i$ levels. These studies emphasize the importance of calcium and gelsolin in the recycling of actin filaments and demonstrate how this activity may complement actin-depolymerizing factor (ADF)/cofilin in remodeling the actin cytoskeleton during nonmuscle cell movement.

Materials and Methods

Materials. Cell biology reagents for cell maintenance were obtained from GIBCO. 1,2-Bis(2-aminophenoxy)ethane-N,N,N',N'-tetraacetate-acetoxymethyl ester (BAPTA-AM) and Fura 2-acetoxymethyl ester (Fura-2-AM) were from Molecular Probes. EGFP–gelsolin cDNA was a gift of Gregor Cicchetti (Harvard University, Boston). Cytoplasmic full-length murine gelsolin cDNA (20) was inserted into pEGFP-N1 (Clontech) as described (21) by using the *Bsp*EI and *Xho*I sites, and the insert was sequenced for sequence verification. Recombinant gelsolin

CELL BIOLOGY

was purified as described (22). Recombinant *Xenopus* ADF/cofilin (XAC) was purified as described (23). All other chemicals were of analytical grade and obtained from Sigma.

Culture of Madin–Darby Canine Kidney (MDCK), PtK2, and Mouse Embryo Fibroblast Cells. MDCK cells stably transfected with EGFP–actin (a kind gift of Beat Imhof, University of Geneva) (24) and PtK2 were cultured as described (17). Gelsolin-null primary mouse embryo fibroblasts were derived from gelsolin-null mice kindly provided by Walter Witke (European Molecular Biology Laboratory, Monterotondo, Italy) (25).

Immunofluorescence Staining of PtK2 Cells and Transfection of PtK2 Cells with EGFP–Gelsolin. Immunofluorescence micrographs were generated with antigelsolin antibody by using standard protocols as described (26). For transfection experiments, EGFP–gelsolin cDNA (2 μg/ml) was added with Lipofectin to PtK2 cells plated on 35-mm Petri dishes by using the manufacturer's protocol.

Infection of Tissue Culture Cells. Both EGFP–actin–MDCK cells and PtK2 cells transfected with EGFP–gelsolin were infected with *Listeria monocytogenes 10403S*, virulent strain serotype-1 as described (17).

Loading of BAPTA-AM into Infected Cells and Measurement of [Ca²⁺]ᵢ. After *Listeria* began moving in the cytoplasm, EGFP–actin–MDCK cells were treated with pluronic acid 127 (0.2 mg/ml) and 40 μM BAPTA-AM for 20–30 min at 25°C in PBS containing 1 mM EGTA and 1 mM MgCl₂. When [Ca²⁺]ᵢ was measured, these same cells were also loaded with 2 μM Fura-2-AM. For measurement of [Ca²⁺]ᵢ, individual cells were monitored by using dual excitation (380 and 340 nm) and a single emission (510 nm) wavelength. Ionomycin combined with calcium was used to determine R_{max} and ionomycin combined with EGTA to determine R_{min}, as described (27).

Microinjection of Gelsolin and XAC. Individual cells were microinjected with gelsolin or XAC as described (28). A needle concentration of 500 nM of each protein in PBS, pH 7.1 was microinjected, resulting in an estimated intracellular concentration of 50 nM (28).

Xenopus Extract Experiments. Extracts were generated as described (29). One hundred microliters of extract (final concentration of 10 mg/ml) was depleted of gelsolin and/or XAC exactly as described (29). After bead absorption, the protein concentrations were identical for specific antibody-depleted and mock-depleted extracts. Depletion was documented by Western blot using a standard protocol (30).

Microscopy and Image Processing. Phase-contrast and fluorescence images of infected cells were obtained with a Nikon Diaphot inverted microscope equipped with a cooled charge-coupled device camera (model C5985, Hamamatsu, Middlesex, NJ) and processed with METAMORPH 4.0 image software (Universal Imaging, West Chester, PA). Depolymerization rates of the actin tails were obtained before and after BAPTA-AM loading by measuring EGFP–actin fluorescence intensity in a single area (5 × 5 pixels) of the tail every 10 s by using the regional measurements function. The relative intensity of an identical area (5 × 5 pixels) on either side of the tail was also measured and subtracted as background from the relative intensity of the tail. *Listeria* velocity measurements were determined as described (28). Statistical analysis was performed by using a two-tailed Wilcoxin nonparametric test.

Results

Length, Assembly, and Disassembly Rates of *Listeria* Actin Tails Before and After BAPTA-AM. We infected MDCK cells stably transfected with EGFP–actin and examined the effects of treatment with BAPTA-AM, the membrane-permeable form of the high-affinity Ca²⁺ chelator BAPTA on *Listeria* actin tail kinetics. By fluorescence microscopy, we noted actin tails behind motile bacteria lengthened ≈3-fold within 15–30 min of BAPTA-AM exposure. Before exposure mean length was 5.8 ± 0.7 μm (SEM, $n = 7$, three separate experiments), and after exposure, tails increased to 16.8 ± 2.2 μm (SEM, $n = 6$, three separate experiments; difference, $P = 0.0012$ by Wilcoxon nonparametric test) (Fig. 1 *A* and *B* and Movies 1 and 2, which are published as supporting information on the PNAS web site). The low relative intensity, as well as thinner dimensions of the distal regions of the tail, compromised accurate assessment of tail length. It is likely that the inability to exactly determine where the tails ended resulted in an underestimation of true length.

Reductions in intracellular calcium had no effect on the trajectory of the bacteria and caused no significant change in mean bacterial velocity, a reflection of actin filament assembly rate (pretreatment: 0.10 ± 0.01 μm/s, $n = 168$; posttreatment: 0.12 ± 0.02 μm/s, $n = 199$; $P = 0.84$, five separate experiments). In some cases BAPTA-AM treatment was associated with a modest increase and in others a slight decrease in velocity. Because velocity was not significantly altered by calcium chelation, a slowing in the rate of actin tail depolymerization was the only other possible explanation for tail lengthening. To confirm this supposition, we measured the relative fluorescence intensity in the same area of the actin tail over time in normal and low-Ca²⁺ conditions in EGFP–actin-transfected MDCK cells. As shown in Fig. 1*C*, the rate of disassembly as assessed by loss of fluorescence was significantly slowed when intracellular Ca²⁺ was lowered by BAPTA-AM treatment. Mean disassembly rates were 29.2 ± 1.5 relative fluorescence units/s ($n = 7$ measurements, three separate experiments) before treatment versus 6.4 ± 1.3 units/s ($n = 7$ measurements, three separate experiments) after BAPTA-AM treatment, $P < 0.001$. During the time frame of our experiments, no significant bleaching of the EGFP was observed ($<5\%$), as assessed by measuring changes in the fluorescence of static actin filament structures.

To assure that our treatment conditions resulted in a significant lowering of [Ca²⁺]ᵢ, *Listeria*-infected cells were loaded with Fura-2-AM before BAPTA-AM loading. The resting free calcium concentration in *Listeria*-infected MDCK cells was 145 ± 11 nM (mean $\pm$ SEM, $n = 83$) and was identical to uninfected cells on the same tissue culture dish (Fig. 1*D*). Despite acquisition of images at 5-s intervals and digital zooming of these images, we could not detect any local changes in [Ca²⁺]ᵢ near the motile bacteria or actin tails. Treatment with BAPTA-AM decreased [Ca²⁺]ᵢ to 37 ± 2 nM (mean $\pm$ SEM, $n = 83$) within 10 min. After replacement of BAPTA-AM with a calcium-free solution containing 1 mM EGTA, the [Ca²⁺]ᵢ continued to decrease, dropping to <20 nM. BAPTA-AM and Fura-2-AM loading were performed at 25°C in all experiments, because at higher temperatures Fura-2-AM was noted to concentrate in cytoplasmic vesicles rather than to evenly distribute in the cytoplasm.

Effects of [Ca²⁺]ᵢ on Localization of EGFP–Gelsolin to Actin Tails. Our experiments demonstrated that depolymerization of actin tails has a calcium-sensitive component. The primary calcium-sensitive actin-severing protein in nonmuscle cells is gelsolin, which has previously been shown to localize to the *Listeria* actin tails by immunofluorescence (26, 29). To investigate the effect of calcium on gelsolin localization, we transfected PtK2 cells with EGFP–gelsolin and infected these cells with *Listeria*. We found
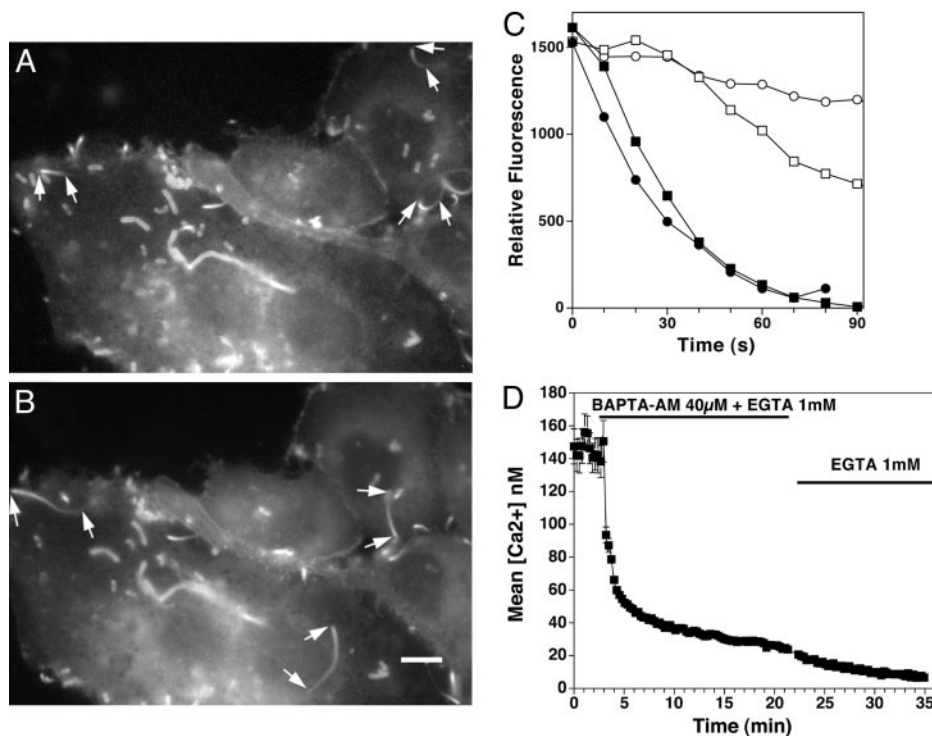
Fig. 1. Effects of BAPTA on *Listeria* actin filament tail length and disassembly rates. (*A*) Actin tails of motile *Listeria* before BAPTA-AM treatment are short. Arrows point to the front (wider end of the tail) and back (narrower end of the tail) of several motile bacteria that cannot be seen in the fluorescent image. Other actin structures remain fixed in the cytoplasm. Some of these structures represent filopodia. Also see Movie 1. (*B*) Actin tails after treatment. The cells shown in *A* were exposed to BAPTA-AM. A dramatic lengthening of the tails was noted within 15–30 min. Also see Movie 2. (Bar: 10 μM.) (*C*) Graph of relative intensity over time of *Listeria* EGFP–actin tails before and after BAPTA-AM treatment. The relative intensity of a discrete area in the tail was measured over time (see *Materials and Methods*). Filled symbols represent depolymerization rates of two different actin tails in untreated cells, and open symbols represent two tails after 15-min exposure to BAPTA-AM. Data are representative of seven different experiments. (*D*) Effects of BAPTA-AM on resting $[Ca^{2+}]_i$ in *Listeria*-infected, EGFP–actin-transfected MDCK cells. Cells were first infected with *Listeria* for 2 h, then loaded with Fura-2-AM for 30 min and exposed to BAPTA-AM at the indicated time. $[Ca^{2+}]_i$ was measured over time as described in *Materials and Methods*. EGTA (1 mM) was kept in the buffer throughout the measurement period. Brackets represent the SEM of 83 determinations.

that EGFP–gelsolin localized to the actin tails in cells with normal calcium concentrations (Fig. 2, Control). However, within 10 min of initiating treatment with BAPTA-AM, EGFP–gelsolin had dissociated from 60% of the actin tails and by 20 min 100% of the *Listeria* tails failed to concentrate EGFP-gelsolin (Fig. 2, BAPTA-AM). Infection of PtK2 cells transfected with EGFP alone did not result in localization of fluorescence to the actin tails in normal or low calcium concentrations (data not
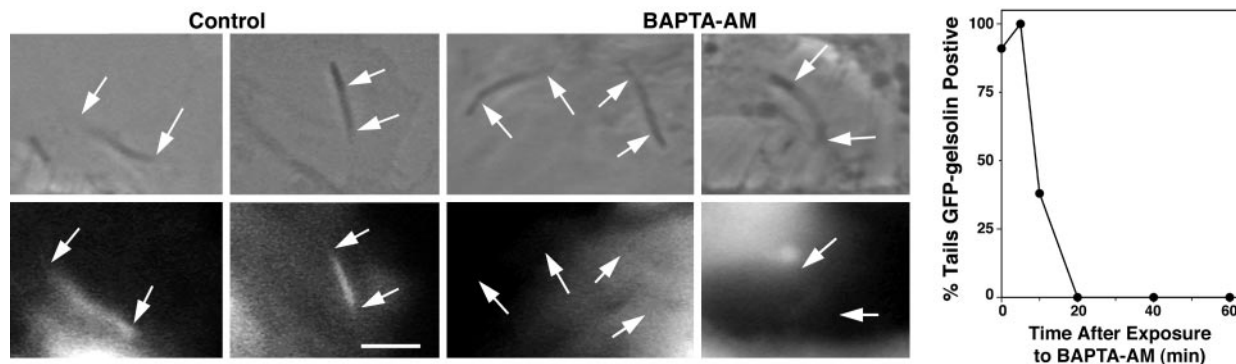

Fig. 2. Effects of BAPTA-AM on gelsolin localization to *Listeria* actin filament tails. Fluorescence micrographs of *Listeria*-infected PtK2 cells transfected with EGFP–gelsolin before and after BAPTA-AM treatment. Simultaneous phase (upper image of each pair) and fluorescence images (lower image of each pair) of *Listeria* actin tails are shown. (Bar: 10 μm.) Arrows point to the beginning and end of each tail as determined by phase microscopy. Actin filaments in the *Listeria* tails often produce phase-dense structures (17). However, these structures do not accurately reflect true tail length, explaining the seemingly comparable lengths of the tails before and after BAPTA-AM treatment. For control, before treatment with BAPTA-AM, EGFP–gelsolin can be seen to be more highly concentrated in the *Listeria* actin tails. Phase density and fluorescence intensity coincide, indicating the presence of gelsolin in the tails. After BAPTA-AM treatment, EGFP–gelsolin no longer concentrates in the phase dense *Listeria* tails. Graph depicts the percentage of *Listeria* phase-dense tails containing EGFP–gelsolin before and at various times after exposure to BAPTA-AM (final concentration, 40 μM) in live PtK2 cells. The number of tails analyzed per time point was as follows: 0 min, 11; 5 min, 8; 10 min, 8; 20 min, 7; 40 min, 4; and 60 min, 4.
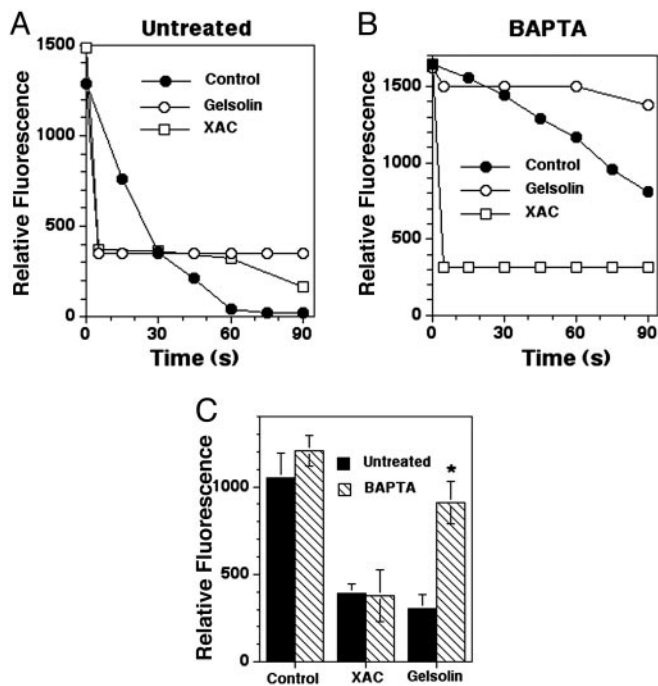
Fig. 3. The effects of microinjecting gelsolin and XAC on *Listeria* tail depolymerization. (*A*) Depolymerization curves of *Listeria* actin tails in untreated EGFP–actin-transfected MDCK cells before (control, ●) and after the microinjection of gelsolin (○) and XAC (□). The estimated final concentration of both proteins was 50 nM (needle concentration, 0.5 μM). Note that within 5 s of injection of both proteins the fluorescence intensity of each *Listeria* actin tail had dropped to its minimum level. (*B*) Depolymerization curves of *Listeria* actin tails in BAPTA-AM-treated, EGFP–actin-transfected MDCK cells before (Control, ●) and after microinjection of the same concentration of gelsolin (○) and XAC (□). In this experiment introduction of gelsolin caused a moderate slowing of the disassembly rate of the tail as compared with uninjected cells. In other experiments a slight, but insignificant, acceleration in disassembly was observed (see *Results*). (*C*) Shown are comparisons of the relative fluorescence intensity of the *Listeria* actin tails at the first measured time point in the depolymerization curves of uninjected cells (T = 0 s) and after microinjection of gelsolin and XAC (T = 5 s). Solid bars indicate no treatment, and hashed bars indicate BAPTA-AM treatment. The difference in mean tail fluorescence intensity between gelsolin-microinjected BAPTA-AM-treated and untreated cells was highly significant (*, P = 0.0006). Brackets represent the SEM of 7–16 determinations (exception, microinjection of XAC in untreated cells, n = 2).

shown). Immunofluorescence staining of *Listeria*-infected PtK2 cells with antigelsolin antibody under normal and low-calcium conditions yielded similar findings (data not shown).

Effects of Microinjection of Gelsolin and XAC on Actin Tails in EGFP–Actin–MDCK Cells. To further explore the role of gelsolin in actin tail disassembly, we compared the severing activity of gelsolin with the primary calcium-independent actin-regulatory protein known to shorten actin filaments, ADF/cofilin (31). Fluorescence decay curves of actin tails were measured before and after microinjection of either gelsolin or XAC into *Listeria*-infected EGFP–actin–MDCK cells in normal and low calcium conditions. Rapid disassembly followed microinjection of 50 nM gelsolin into untreated cells (mean disassembly rate, 150 units per s, n = 7) (Fig. 3*A*). At the first time point that could be measured (5 s) the fluorescence intensity had already plateaued, remaining constant over 2 min. However, when the same concentration of gelsolin was microinjected into BAPTA-AM-treated cells, gelsolin minimally accelerated or slightly slowed disassembly (mean disassembly rate, 3.4 units per s, n = 3 after

gelsolin microinjection vs. 6.8 units per s before microinjection, n = 3) (Fig. 3*B*). In contrast, microinjection of 50 nM XAC into *Listeria*-infected EGFP–actin–MDCK cells resulted in enhanced actin tail disassembly in both untreated (mean rate: 132 units per s, n = 2) and BAPTA-AM-treated cells (mean rate: 165 units per s, n = 9) (Fig. 3 *A* and *B*). Comparisons of the mean fluorescence intensities of *Listeria* actin tails at the first measurable time point in each depolymerization curve (5 s) revealed similar intensities for untreated cells microinjected with gelsolin and XAC. However, after BAPTA-AM treatment tails in cells microinjected with gelsolin had significantly higher fluorescence intensities than cells microinjected with XAC (P = 0.03) or untreated cells microinjected with gelsolin (P = 0.0006) (Fig. 3*C*).

Effects of [Ca²⁺]ᵢ on *Listeria* Tail Lengths in *Xenopus* Extracts. The effects of lowering $[Ca^{2+}]_i$ on *Listeria* actin tail length was also examined in *Xenopus* extracts. As observed in intact cells, low-calcium conditions resulted in long actin tails, whereas in extracts containing higher $[Ca^{2+}]$ (estimated concentration 40 μM), *Listeria* formed very short tails (See Fig. 4 *B* and *C*). To explore the contribution of gelsolin and XAC to this calcium-sensitive shortening, we compared gelsolin and XAC immuno-depleted to mock-depleted *Xenopus* extracts (see *Materials and Methods*). Western blot analysis revealed that immunodepletion reduced gelsolin and XAC content to undetectable levels (Fig. 4*A*). In extracts containing EGTA, *Listeria* actin tails in gelsolin-depleted extracts were slightly longer than control extracts; however, this difference was not statistically significant (P > 0.05). Under the same low-calcium condition, depletion of XAC was associated with a doubling of tail length as compared with control extract (Fig. 4 *B* and *C*). These observations agree with previous studies (29). Addition of $CaCl_2$ to control and XAC-depleted extracts to achieve a final $[Ca^{2+}]$ of 40 μM caused a marked shortening of *Listeria* actin tail lengths (P < 0.0001) (Fig. 4 *B* and *C*). Analysis of >20 images by a blinded observer failed to detect any systematic differences in the morphology of tails formed in XAC-depleted extract as compared with those formed in mock-depleted extract. Addition of the same concentration of $CaCl_2$ to gelsolin-depleted extract minimally affected tail length, and the differences in tail length between high and low Ca^{2+} conditions were not statistically significant (P = 0.19) (Fig. 4 *B* and *C*). When gelsolin was added back to the gelsolin-depleted extract (final concentration 50 nM) calcium-sensitive tail shortening was restored, mean lengths being similar to control extracts (mean length 7.2 ± 2.3 μm in gelsolin-depleted extract plus purified gelsolin vs. 5.7 ± 1.3 μm for mock-depleted extract). Finally, extracts were depleted of both XAC and gelsolin. Tail lengths were not significantly different than observed for XAC depletion alone in EGTA, but failed to shorten on addition of calcium (mean tail length 69.5 ± 9 μm before vs. 71.6 ± 7.2 μm after addition of calcium).

Effects of BAPTA-AM Treatment on *Listeria* Tail Lengths in Gelsolin-Null Cells. To definitively prove that gelsolin was required for *in vivo* calcium-sensitive shortening of *Listeria* tails, we infected gelsolin-null mouse embryo fibroblasts. Before treatment actin filament tail lengths were significantly longer in gelsolin-null cells as compared with WT cells. As observed in gelsolin-depleted *Xenopus* extracts, the calcium-sensitive effect on tail length was not seen in gelsolin-null cells. Rather than increasing tail length, addition of BAPTA-AM to *Listeria*-infected gelsolin-null cells resulted in a slight, statistically insignificant shortening of mean tail length (P > 0.05); whereas the same treatment of WT mouse embryo fibroblast cells resulted in a doubling of mean tail length (Fig. 5).
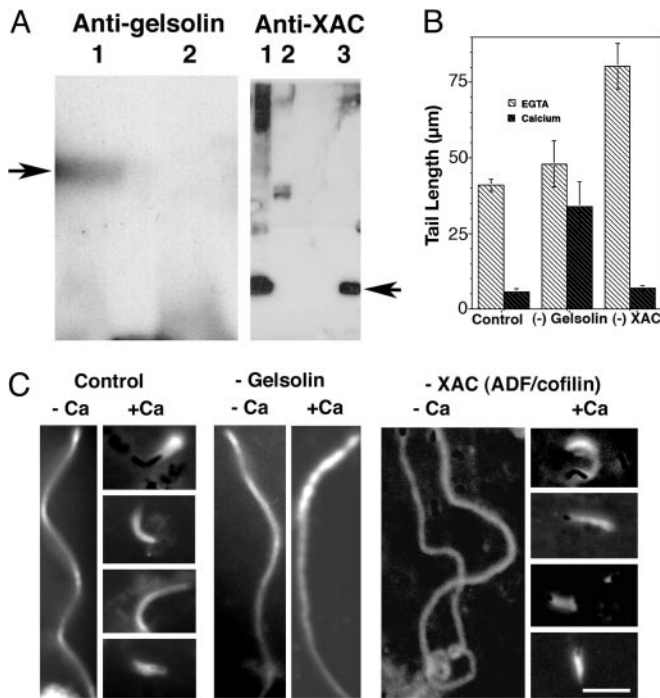
Fig. 4. The effects of low and high $[Ca^{2+}]_i$ on *Listeria* actin tail length in *Xenopus* extracts before and after gelsolin immunodepletion and after the readdition of purified gelsolin. (*A*) Western blots of *Xenopus* extracts are shown. (*Left*) Mock-depleted extract (lane 1) and gelsolin immuno-depleted extract (lane 2) were prepared with polyclonal goat antigelsolin antibody. The arrow points to the expected molecular weight of purified gelsolin. (*Right*) Mock-depleted extract (lane 1) and XAC immuno-depleted *Xenopus* extract (lane 2) were prepared with polyclonal rabbit anti-XAC1 and anti-XAC2 antibody. Purified XAC (lane 3). The arrow points to the expected molecular weight of XAC. (*B*) Shown is a comparison of *Listeria* actin tail lengths in mock-depleted extracts (Control), gelsolin-depleted extracts (−Gelsolin), and XAC-depleted extracts (−XAC), in EGTA buffer (light hashed bars) before and after the addition of 1 mM CaCl$_2$ (dark hashed bars), calculated free calcium concentration 40 μM. The mean tail lengths for each extract were as follows: control, low $[Ca^{2+}]$, 41.3 ± 3.3 μm, $n = 11$ vs. high $[Ca^{2+}]$, 5.6 ± 1.3 μm, $n = 14$, $P < 0.0001$; gelsolin-depleted: low $[Ca^{2+}]$, 48.5 ± 7.6 μm, $n = 18$ vs. high $[Ca^{2+}]$, 33.9 ± 8.2 μm, $n = 14$, $P = 0.19$; XAC-depleted low $[Ca^{2+}]$, 80.3 ± 7.6, $n = 44$ vs. high $[Ca^{2+}]$ 6.9 ± 0.5 μm, $n = 48$, $P < 0.0001$. (*C*) Shown are representative fluorescence micrographs of rhodamine-labeled actin in *Xenopus* extracts (see *Materials and Methods*). Control −Ca indicates mock-depleted extract containing 1 mM EGTA; Control +Ca indicates mock-depleted extract containing 1 mM EGTA and 1 mM CaCl$_2$. For −Gelsolin, −Ca indicates gelsolin-depleted extract containing 1 mM EGTA; +Ca indicates gelsolin-depleted extract containing 1 mM EGTA and 1 mM CaCl$_2$. For −XAC, −Ca indicates XAC-depleted extract containing 1 mM EGTA; +Ca indicates XAC-depleted extract containing 1 mM EGTA and 1 mM CaCl$_2$. (Bar: 10 μm.)

Fig. 5. The effects of BAPTA-AM treatment on *Listeria* tail lengths in WT and gelsolin-null mouse embryo fibroblasts are compared. Cells were infected with *Listeria*, and, 4–5 h after the initiation of infection, cells were formalin-fixed, Triton-permeabilized, and stained with Alexa-phalloidin as described in *Materials and Methods*. *Listeria* actin tail lengths were measured for each condition. (*Left*) Bars represent the SEM of $n = 68$–91 measurements. (*Right*) Fluorescence micrographs show typical examples of Alexa-phalloidin-stained gelsolin-null cells infected with *Listeria* before and after BAPTA-AM treatment. Western blot analysis confirmed that the gelsolin-null cells contained no detectable gelsolin (data not shown).

Discussion

The effects of calcium on *Listeria*-induced actin assembly and disassembly have not been previously studied to our knowledge. In agreement with previous studies of agonist-induced actin assembly in neutrophils and macrophages, we find that reductions in cytoplasmic $[Ca^{2+}]$ fail to inhibit *Listeria*-induced actin assembly. In contrast, reductions in intracellular $[Ca^{2+}]$ markedly affect the recycling of actin tails, dramatically lowering their disassembly rates. Depolymerization rates of actin filament tails slowed to one-quarter of those observed in cells with normal $[Ca^{2+}]_i$. This slowing of the disassembly rates of *Listeria* actin tails was a consistent finding. One previous study of neutrophils found an increase in the thickness of actin filament structures surrounding phagolysosomes after $[Ca^{2+}]_i$ chelation, a finding that is also consistent with a slowing of actin disassembly (32).
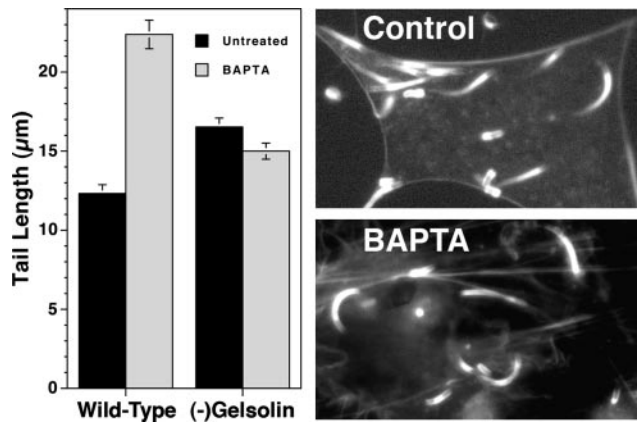
In glass-adherent platelets reductions of intracellular calcium are associated with the lengthening of actin filaments within platelet filopods, indicating that platelets also possess a calcium-sensitive actin recycling activity (12).

The most likely protein to mediate calcium-sensitive disassembly is gelsolin (33). Previous studies have demonstrated that loss of gelsolin results in reduced motility of neutrophils and fibroblasts, as well as defective platelet function (25). In addition, actin filament turnover is slower in gelsolin-null as compared with WT fibroblasts and faster in motile cells expressing high levels of gelsolin (34). Overexpression of gelsolin in fibroblasts results in increased chemotaxis (35) and an increase in the velocity of *Listeria* intracellular actin-based motility (26). Immunofluorescence microscopy reveals that gelsolin concentrates along the actin filament tails of intracellular *Listeria*, placing this severing protein in the ideal location for accelerating the disassembly of these actin structures (26, 29). Similarly, we find that EGFP–gelsolin localizes to *Listeria* tails (Fig. 2). When $[Ca^{2+}]_i$ is lowered by BAPTA-AM, EGFP–gelsolin dissociates from the tails. Furthermore, comparisons of the severing activity of microinjected gelsolin and XAC, the primary calcium-insensitive actin filament severing protein involved in the recycling of *Listeria* actin tails (29), reveal that both proteins accelerate actin tail disassembly in cells with normal $[Ca^{2+}]_i$; however, when $[Ca^{2+}]_i$ is reduced, only XAC maintains recycling activity (Fig. 3). Our experiments with *Xenopus* extracts demonstrate that gelsolin recycles actin filaments in *Listeria* tails. Previous studies have emphasized the importance of ADF/cofilin for actin filament recycling (31, 36), and this protein, like gelsolin, localizes to *Listeria* tails (29). Earlier experiments examining the effects of immunodepletion of ADF/cofilin and gelsolin from *Xenopus* extracts, concluded that ADF/cofilin, but not gelsolin was critical for *Listeria* actin tail recycling. This conclusion was based on experiments performed in low $[Ca^{2+}]$, a condition expected to inactivate gelsolin (29). We now show that when calcium is added to *Xenopus* extracts *Listeria* actin tails are markedly shortened. Furthermore, we find that immunodepletion of gelsolin eliminates this calcium-sensitive actin filament shortening activity, whereas immunodepletion of ADF/cofilin does not (Fig. 4). Our experiments with gelsolin-null cells

CELL BIOLOGY

provide proof that gelsolin plays a primary role in calcium-sensitive actin filament recycling. In cells lacking gelsolin, *Listeria* actin tail length is unaffected by calcium chelation (Fig. 5). These experiments also indicate that gelsolin exclusively accounts for *Listeria* actin tail shortening and suggest that mouse embryo fibroblasts do not express other calcium-sensitive actin severing/depolymerizing proteins.

Although *Listeria* infection does not exactly recapitulate the biochemical events associated with chemotaxis and phagocytosis, these experiments strongly support a central role for gelsolin in the recycling of actin filaments. Gelsolin and ADF/cofilin are likely to play complementary roles. Each protein is regulated by both common and distinctly different signals, gelsolin being regulated by phosphoinositides and pH, in addition to calcium (37, 38), and ADF/cofilin by phosphoinositides, pH, and through phosphorylation by LIM kinase (39, 40). These similarities and differences could allow motile cells to coordinately regulate both proteins or activate each protein at different times and in different locations to orchestrate the complex geometric changes in the actin cytoskeleton required for amoeboid movement, phagocytosis, cell spreading, and cell division. Future studies should focus on the signal cascades of each of these motile processes and their impact on gelsolin and ADF/cofilin function.

Our studies of intact host cells raise two other important issues. We show that *Listeria* is able to activate gelsolin deep within the cytoplasm of cells with $[Ca^{2+}]_I$ of 145 nM. However, *in vitro* gelsolin requires μM $[Ca^{2+}]$ to function (41). How is *Listeria* accomplishing this task? Intracellular *Listeria* is able to attract both PI(4,5)P$_2$ and PI(3,4,5)P$_3$ (44), raising the possibility that these phospholipids could serve as substrates for byproducts that locally release intracellular calcium stores. Alternatively, these phosphoinositides could serve as docking sites for a kinase or kinases that activate gelsolin. Consistent with this latter mechanism, tyrosine phosphorylation has been shown to activate severing by the gelsolin family member villin in low Ca^{2+} solutions (42). Our work raises another important question. What mechanism allows gelsolin to turn over actin filament subunits so quickly in the presence of calcium? *In vitro*, purified gelsolin severs and caps actin filaments; however, *in vivo* gelsolin must dissociate from the filament ends to efficiently promote filament recycling. Phosphoinositides (37) and tropomyosin (43) are both present in *Listeria* actin tails (17) and could mediate gelsolin uncapping. Further exploration of the pathways that regulate gelsolin activity during *Listeria* actin-based motility promises to provide additional clues as to how gelsolin functions in living cells to recycle actin filaments during cell movement.

1. Yin, H. L. & Stossel, T. P. (1979) *Nature* **281,** 583–586.
2. Condeelis, J. (1993) *Annu. Rev. Cell Biol.* **9,** 411–444.
3. Stossel, T. P. (1993) *Science* **260,** 1086–1094.
4. White, J. R., Naccache, P. H. & Sha'afi, R. I. (1983) *J. Biol. Chem.* **258,** 14041–14047.
5. Wallace, P. J., Wersto, R. P., Packman, C. H. & Lichtman, M. A. (1984) *J. Cell Biol.* **99,** 1060–1065.
6. Howard, T. H. & Oresajo, C. O. (1985) *J. Cell Biol.* **101,** 1078–1085.
7. Sklar, L. A. & Oades, Z. G. (1985) *J. Biol. Chem.* **260,** 11468–11475.
8. Lew, P. D., Wollheim, C. B., Waldvogel, F. A. & Pozzan, T. (1984) *J. Cell Biol.* **99,** 1212–1220.
9. Meshulam, T., Proto, P., Diamond, R. D. & Melnick, D. A. (1986) *J. Immunol.* **137,** 1954–1960.
10. Carson, M., Weber, A. & Zigmond, S. H. (1986) *J. Cell Biol.* **103,** 2707–2714.
11. Greenberg, S., el Khoury, J., di Virgilio, F., Kaplan, E. M. & Silverstein, S. C. (1991) *J. Cell Biol.* **113,** 757–767.
12. Hartwig, J. H. (1992) *J. Cell Biol.* **118,** 1421–1442.
13. Cossart, P. (1995) *Curr. Opin. Cell Biol.* **7,** 94–101.
14. Wadsworth, S. J. & Goldfine, H. (1999) *Infect. Immun.* **67,** 1770–1778.
15. Dramsi, S. & Cossart, P. (2003) *Infect. Immun.* **71,** 3614–3618.
16. Cossart, P. & Sansonetti, P. J. (2004) *Science* **304,** 242–248.
17. Dabiri, G. A., Sanger, J. M., Portnoy, D. A. & Southwick, F. S. (1990) *Proc. Natl. Acad. Sci. USA* **87,** 6068–6072.
18. Sanger, J. M., Sanger, J. W. & Southwick, F. S. (1992) *Infect. Immun.* **60,** 3609–3619.
19. Theriot, J. A., Mitchison, T. J., Tilney, L. G. & Portnoy, D. A. (1992) *Nature* **357,** 257–260.
20. Kwiatkowski, D. J., Stossel, T. P., Orkin, S. H., Mole, J. E., Colten, H. R. & Yin, H. L. (1986) *Nature* **323,** 455–458.
21. De Corte, V., Bruyneel, E., Boucherie, C., Mareel, M., Vandekerckhove, J. & Gettemans, J. (2002) *EMBO J.* **21,** 6781–6790.
22. Southwick, F. S. (1995) *J. Biol. Chem.* **270,** 45–48.
23. Abe, H., Obinata, T., Minamide, L. S. & Bamburg, J. R. (1996) *J. Cell Biol.* **132,** 871–885.
24. Ballestrem, C., Wehrle-Haller, B. & Imhof, B. A. (1998) *J. Cell Sci.* **111,** 1649–1658.
25. Witke, W., Sharpe, A. H., Hartwig, J. H., Azuma, T., Stossel, T. P. & Kwiatkowski, D. J. (1995) *Cell* **81,** 41–51.
26. Laine, R. O., Phaneuf, K. L., Cunningham, C. C., Kwiatkowski, D., Azuma, T. & Southwick, F. S. (1998) *Infect. Immun.* **66,** 3775–3782.
27. Demaurex, N., Schlegel, W., Varnai, P., Mayr, G., Lew, D. P. & Krause, K. H. (1992) *J. Clin. Invest.* **90,** 830–839.
28. Zeile, W. L., Purich, D. L. & Southwick, F. S. (1996) *J. Cell Biol.* **133,** 49–59.
29. Rosenblatt, J., Agnew, B. J., Abe, H., Bamburg, J. R. & Mitchison, T. J. (1997) *J. Cell Biol.* **136,** 1323–1332.
30. Laine, R. O., Zeile, W., Kang, F., Purich, D. L. & Southwick, F. S. (1997) *J. Cell Biol.* **138,** 1255–1264.
31. Bamburg, J. R. (1999) *Annu. Rev. Cell Dev. Biol.* **15,** 185–230.
32. Bengtsson, T., Jaconi, M. E., Gustafson, M., Magnusson, K. E., Theler, J. M., Lew, D. P. & Stendahl, O. (1993) *Eur. J. Cell Biol.* **62,** 49–58.
33. Kwiatkowski, D. J. (1999) *Curr. Opin. Cell Biol.* **11,** 103–108.
34. McGrath, J. L., Osborn, E. A., Tardy, Y. S., Dewey, C. F., Jr. & Hartwig, J. H. (2000) *Proc. Natl. Acad. Sci. USA* **97,** 6532–6537.
35. Cunningham, C. C., Stossel, T. P. & Kwiatkowski, D. J. (1991) *Science* **251,** 1233–1236.
36. Carlier, M. F., Laurent, V., Santolini, J., Melki, R., Didry, D., Xia, G. X., Hong, Y., Chua, N. H. & Pantaloni, D. (1997) *J. Cell Biol.* **136,** 1307–1322.
37. Janmey, P. A. & Lindberg, U. (2004) *Nat. Rev. Mol. Cell. Biol.* **5,** 658–666.
38. Allen, P. G., Laham, L. E., Way, M. & Janmey, P. A. (1996) *J. Biol. Chem.* **271,** 4665–4670.
39. Arber, S., Barbayannis, F. A., Hanser, H., Schneider, C., Stanyon, C. A., Bernard, O. & Caroni, P. (1998) *Nature* **393,** 805–809.
40. Yang, N., Higuchi, O., Ohashi, K., Nagata, K., Wada, A., Kangawa, K., Nishida, E. & Mizuno, K. (1998) *Nature* **393,** 809–812.
41. Janmey, P. A., Chaponnier, C., Lind, S. E., Zaner, K. S., Stossel, T. P. & Yin, H. L. (1985) *Biochemistry* **24,** 3714–3723.
42. Kumar, N. & Khurana, S. (2004) *J. Biol. Chem.* **279,** 24915–24918.
43. Nyakern-Meazza, M., Narayan, K., Schutt, C. E. & Lindberg, U. (2002) *J. Biol. Chem.* **277,** 28774–28779.
44. Sidhu, G., Li, W., Laryngakis, N., Bishai, E., Balla, T. & Southwick, F. S. (2005) *J. Biol. Chem.*, in press.